Pedersen, R.B., Christie, D.M., and Miller, D.J. (Eds.)
Proceedings of the Ocean Drilling Program, Scientific Results Volume 187

3. Regional and Local Mantle Heterogeneities Associated with the Australian Antarctic Discordance: Sr and Nd Isotopic Results from ODP Leg 187[1]

Rolf B. Pedersen,[2] David M. Christie,[3] and Douglas G. Pyle[4]

ABSTRACT

The principal objective of Leg 187 was to locate the Indian/Pacific mantle boundary by sampling and analyzing 8- to 28-Ma seafloor basalts to the north of the Australian Antarctic Discordance (AAD). In this paper we present Sr and Nd isotopic data from basaltic glasses recovered from the 13 sites drilled during Leg 187. Our data show that the boundary region is characterized by a gradual east-west increase in $^{87}Sr/^{86}Sr$, with a corresponding decrease in $^{143}Nd/^{144}Nd$ across a 150-km-wide zone located east and west of the 127°E Fracture Zone. The Sr-Nd isotopic composition of glasses therefore confirms the general conclusions derived by the Leg 187 shipboard scientific party in that the mantle boundary follows a west-pointing, V-shaped depth anomaly that stretches across the ocean floor from the Australian to the Antarctic continental margins.

We document that two systematic trends of covariation between $^{87}Sr/^{86}Sr$ and $^{143}Nd/^{144}Nd$ can be distinguished, suggesting that the basalts sampled during Leg 187 formed through the interaction of three contrasting source components: (1) a component that lies within the broad spectrum of Indian-type mantle compositions, (2) a boundary component, and (3) a Pacific-type mantle component. The variations in elemental and isotopic compositions indicate that the boundary component represents a distinct mantle region that is associated with the

[1]Pedersen, R.B., Christie, D.M., and Pyle, D.G., 2004. Regional and local mantle heterogeneities associated with the Australian Antarctic Discordance: Sr and Nd isotopic results from ODP Leg 187. *In* Pedersen, R.B., Christie, D.M., and Miller, D.J. (Eds.), *Proc. ODP, Sci. Results,* 187, 1–23 [Online]. Available from World Wide Web: <http://www-odp.tamu.edu/publications/187_SR/VOLUME/CHAPTERS/205.PDF>. [Cited YYYY-MM-DD]
[2]Department of Earth Science, University of Bergen, Allegaten 41, N-5007 Bergen, Norway.
rolf.pedersen@geo.uib.no
[3]College of Oceanic and Atmospheric Sciences, Oregon State University, 104 Ocean Administration Building, Corvallis OR 97331-5503, USA.
[4]Department of Geology and Geophysics, SOEST, University of Hawaii, 1680 East-West Road, Honolulu HI 96822, USA.

Initial receipt: 7 November 2003
Acceptance: 1 September 2004
Web publication: 2 November 2004
Ms 187SR-205

boundary between the Pacific and the Indian mid-ocean-ridge basalt (MORB) sources rather than a dispersed mantle heterogeneity that was preferentially extracted in the boundary region. However, the origin of the boundary component remains an open question. The three components are not randomly intermixed. The Indian and the Pacific mantle sources both interacted with the boundary component, but they seem not to have interacted directly with each other. Large local variability in isotopic compositions of lavas from the mantle boundary region demonstrates that magma extraction processes were unable to homogenize the isotopic contrasts present in the mantle source in this region.

Systematic variations in rare earth element (REE) concentrations across the depth anomaly cannot be explained solely by variations in source composition. The observed variations may be explained by an eastward increase and westward decrease in the degree of melting toward the mantle boundary region, compatible with a cooling of the Pacific mantle and a heating of the Indian mantle toward the mantle boundary.

INTRODUCTION

The Australian Antarctic Discordance (AAD) is located on the Southeast Indian Ridge (SEIR) and is one of the deepest parts of the global mid-ocean-ridge system (4000–5000 m). This unusual deep 500-km section of the ridge is located at the center of a basin-wide seafloor depression between Australia and Antarctica that appears to have existed in this region since seafloor spreading began at ~100 Ma (Fig. **F1**). This depth anomaly exhibits a broad V-shaped pattern, suggesting that the deep part of the ridge has migrated westward at a rate of 15 mm/yr (Marks et al., 1990, 1991). A regional geoid low (Weissel and Hayes, 1971) and anomalously high upper mantle shear wave velocities are associated with the depth anomaly, indicating the presence of cooler mantle beneath the AAD (Forsyth et al., 1987).

Marked differences in the seafloor morphology along the ridge probably reflect this difference in mantle temperature (Fig. **F2**). Despite a regionally uniform spreading rate of ~74 mm/yr, the morphology changes from a smooth topography typical of fast-spreading ridges east of the AAD (Zone A) to a deep axial valley and rough off-axis topography typical of slow-spreading ridges within the AAD (Zone B) (see Figs. **F1** and **F3** for how the zones in the AAD region are defined). These morphologic changes probably reflect fundamental differences in magma supply rates beneath adjacent portions of the ridge. The low magma supply in the AAD region is also suggested to be responsible for other anomalous characteristics such as unusually thin oceanic crust and chaotic seafloor terrain dominated by listric extensional faulting (Christie et al., 1998).

The eastern boundary of the AAD, located at the 127°E ridge-transform intersection, exhibits distinct contrasts in the nature and variability of basaltic compositions (Pyle, 1994). Relative to Zone A lavas, the AAD lavas are generally more primitive and have Na, Fe, and Si contents indicating lower extents of partial melting and lower mean pressure of melting beneath the AAD.

A boundary between the isotopically distinct Indian and Pacific mid-ocean-ridge basalt (MORB) (Hamelin and Allègre, 1985; Mahoney et al., 1992, 1996) occurs beneath the AAD (Klein et al., 1988; Pyle et al., 1990, 1992). Along the spreading axis the boundary is located

F1. Regional map of the Southern Ocean, p. 13.

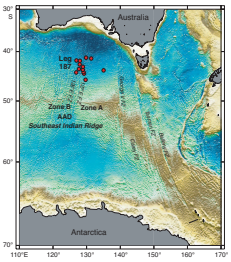

F2. Sites in relation to residual depth anomaly and SeaBeam bathymetry, p. 14.

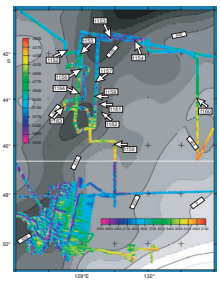

F3. Site locations in relation to seafloor isochrons, p. 15.

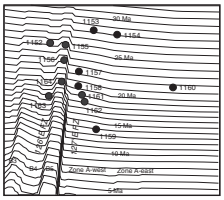

within 20–30 km of the 126°E transform, which defines the western boundary of Zone B5 (Fig. F3). Off-axis dredge sampling has demonstrated that the boundary has migrated westward across Segment B5 during the last 3–4 m.y. at a rate of 25–40 mm/yr (Pyle et al., 1990, 1992; Christie et al., 1998).

The principal objective of Leg 187 was to locate the Indian/Pacific mantle boundary by sampling and analyzing 8- to 28-Ma seafloor basalts to the north of the AAD. In this paper we present Sr and Nd isotopic data from basaltic glasses recovered from the 13 sites drilled during Leg 187 in order to document regional and local mantle heterogeneities associated with the Australian Antarctic Discordance.

LEG 187 DRILLING RESULTS

During Leg 187, 617 m of volcanic basement was drilled at 13 sites, recovering 137 m of core consisting primarily of basalt and basalt rubble. The positions of the drill sites relative to seafloor isochrons show that the seafloor sampled ranges in age from 14 to 28 Ma (Fig. F3). Eight sites (1153, 1154, and 1157–1162) were drilled in Zone A, three sites (1154, 1155, and 1164) were drilled in Segment B5, between the 126°E and the 127°E Fracture Zones, and two sites (1152 and 1163) were drilled west of the 126°E Fracture Zone in Segment B4.

All holes were relatively shallow, typically 20–50 m into volcanic basement with a maximum penetration of 66 m (Hole 1164B). The dominant lithology recovered was pillow basalt, either as pillow flows or basaltic rubble. Basaltic breccias cemented by carbonates, clays, and lithic debris are also common in the cores. Massive basalts interlayered with pillow basalts were recovered from Site 1160. Hole 1162A is anomalous, as greenschist facies diabase and cataclasite were recovered as clasts in a dolomite-cemented lithic breccia, suggesting that deeper crustal levels were exposed nearby. Only the uppermost volcanic carapace was sampled in all other holes. Basaltic rubble was recovered from 10 of 23 holes, and in these cases primary magmatic stratigraphy cannot be reliably inferred from the relative positions of individual pieces in the core barrel.

Leg 187 basalts range from aphyric to moderately plagioclase and olivine phyric. Clinopyroxene phenocrysts are present only in Holes 1152B and 1164A, both of which are located west of the 127°E Fracture Zone. Chilled margins with basaltic glass are common in most cores.

Handpicked basaltic glasses were analyzed for major and some trace elements by inductively coupled plasma–atomic emission spectroscopy (ICP-AES) onboard the *JOIDES Resolution* during the leg. These analyses were essential for a responsive drilling strategy in which shipboard analyses from each site were used to guide the selection of subsequent sites. The onboard analyses show that the Leg 187 glasses are relatively primitive, with MgO ranging from 9.4 to 7.2 wt%. The analyses also show significant differences in parental magma composition between Leg 187 lavas and lavas from the equivalent segments at the axis of spreading. Particular attention was paid to the Ba and Zr analyses since these elements discriminate well between Indian- and Pacific-type mantle sources for on-axis and near-axis (0–7 Ma) dredge samples (Christie, Pedersen, Miller, 2001). Based on these analyses the shipboard scientific party concluded that (1) no Indian-type mantle occurs east of the –500-m contour on the regional depth anomaly; (2) Pacific- and Transitional-Pacific-type mantle occurs sporadically throughout the eastern region

of the depth anomaly (approximately to the east of the mid-line); and (3) between ~25 and ~14 Ma, Indian- and Pacific-type mantle alternated in Zone A-west on a timescale of a few million years.

Kempton et al. (2002) reported an extensive suite of new Nd, Pb, and Hf isotopic data for basaltic whole-rock and some glass samples from Leg 187, supplemented by near-zero-age samples from the 1976 Vema dredges reported by Klein et al. (1988). They showed that basalts derived from Indian and Pacific MORB mantle sources in the AAD and Zone A can be effectively discriminated using Nd and Hf isotope systematics. Based on this discriminant, Kempton et al. (2002) assigned each Leg 187 drill site to a mantle isotopic domain. These assignments differed from the assignments made by the shipboard party at only two sites and have no effect on the inferred location of the Indian/Pacific mantle boundary.

SAMPLING AND ANALYTICAL METHODS

Samples of chilled margins were carefully crushed in an alumina mortar and sieved to a 1- to 2-mm fraction, washed with nanopure H_2O in an ultrasonic bath for ~30 min, and dried in an oven at 80°–100°C. Approximately 100 mg fresh shiny black basalt glass was then hand-separated from altered material, minerals, whole-rock chips, and spherulitic microcrystalline material under a binocular microscope. Nd and Sr isotopic compositions were measured at the University of Bergen on a Finnigan 262 thermal ionization mass spectrometer (TIMS). Samples were cleaned in 2-M HCl and dissolved in a mixture of HF and HNO_3. Sr and rare earth elements (REEs) were separated by specific-extraction chromatography. Sm and Nd were subsequently separated using HDEHP-coated Teflon powder as the ion-exchange resin. Sr and Nd were loaded onto a double filaments and analyzed in static and dynamic modes, respectively. Sr isotopic ratios are reported relative to Standard Reference Material (SRM) 987 $^{87}Sr/^{86}Sr$ value of 0.710240. Nd isotopic ratios were corrected for mass fractionation using a $^{146}Nd/^{144}Nd$ value of 0.7219. Sm and Nd concentrations were determined using a mixed $^{150}Nd/^{149}Sm$ spike. Repeated measurements of Johnson and Matthey NdO_3 batch number S819093A at the time of the analyses yielded an average $^{143}Nd/^{144}Nd$ ratio of $^{143}/^{144}Nd$ of 0.511115 (±13), which corresponds to a La Jolla value of 0.511851.

RESULTS

A total of 28 samples were analyzed for this study, and the results are listed in Table **T1.** The $^{87}Sr/^{86}Sr$ isotopic ratios of the analyzed glasses range from 0.70253 to 0.70312. The within-site range varies significantly, with the largest local variability at Site 1157, where $^{87}Sr/^{86}Sr$ ranges from 0.70260 to 0.70295, which is 54% of the total range seen in all the sites. Both average and maximum $^{87}Sr/^{86}Sr$ ratios increase systematically from east to west (Fig. **F4**). There is a systematic increase in $^{87}Sr/^{86}Sr$ over at least 200–300 km across the westernmost part of Zone A and Segment B5 to a maximum in Segment B4. The largest within-site variability occurs within the area of the strongest regional gradient in Sr isotopic compositions.

T1. Nd and Sr isotopic compositions, and Nd and Sm, p. 22.

F4. $^{87}Sr/^{86}Sr$, ε_{Nd}, ε_{Hf}, and $^{206}Pb/^{204}Pb$ values, p. 16.

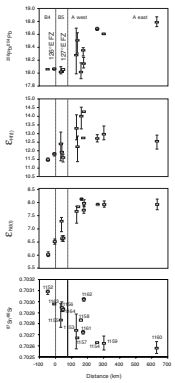

The $^{143}Nd/^{144}Nd$ isotopic ratios range from 0.513069 to 0.512953, corresponding to $\varepsilon_{Nd(t)}$ values from 8.18 to 5.96. There is a systematic westward decrease in ratios, generally paralleling the increase in $^{87}Sr/^{86}Sr$. As for $^{87}Sr/^{86}Sr$, the largest within-site range occurs at Site 1157 where $^{143}Nd/^{144}Nd$ varies from 0.513049 to 0.513015, which is 30% of the total range for all sites. One sample from Site 1162 is anomalous in $^{87}Sr/^{86}Sr$, for which it plots well above the regional trend, but not in $^{143}Nd/^{144}Nd$.

The Sm/Nd of the analyzed glasses ranges from 0.195 to 0.239 and decreases from east to west with by far the largest local variability at Site 1160 (Fig. **F5**). There is also significant within-site variability at sites in Segment B5. Nd contents of the lavas vary from 3.8 to 15.2 ppm. Site 1160 lavas have significantly lower Nd contents than those at the other sites, for which the lowest values are found within Zone B5, whereas the minimum and mean values at each site increase in both directions away from this zone (Fig. **F5**).

Two systematic trends of covariation between Sr and Nd isotopic ratios can be distinguished (Fig. **F6**). Sites in Zone B, west of the 127°E Fracture Zone, yielded glasses with Sr and Nd isotopic compositions that plot along a well-defined negative trend (hereafter termed the "western trend"). Site 1152, the westernmost site (in distance from the 127°E Fracture Zone), defines the high $^{87}Sr/^{86}Sr$–low $^{143}Nd/^{144}Nd$ end-member, and Site 1155, which is located in Zone B5, defines the low $^{87}Sr/^{86}Sr$–high $^{143}Nd/^{144}Nd$ end-member of this trend.

Glasses from sites that are east of the 127°E Fracture Zone define a flat-lying trend with relatively invariant $^{143}Nd/^{144}Nd$ ("eastern trend"). Site 1160, which is the easternmost drilled site, defines the low $^{87}Sr/^{86}Sr$ end-member, and Site 1162, in Zone A-west defines the high $^{87}Sr/^{86}Sr$ end-member of this trend. The glass of this sample contained spherulites, and although the sample was carefully picked and leached before dissolution, it can not be excluded that the relative high $^{87}Sr/^{86}Sr$ of this sample results from low-temperature seawater alteration. Site 1161 has lower $^{87}Sr/^{86}Sr$ than Site 1162 and plots at the intersection of the two trends. Site 1157, which yielded both Indian-type and Pacific-type lavas (Kempton et al., 2002) shows the largest within-site isotopic range. Samples from this site plot on both the eastern and western trends; there is one glass sample clearly associated with each trend and two plotting close to the intersection.

The Leg 187 glasses also define two trends on a $^{143}Nd/^{144}Nd$ vs. $^{147}Sm/^{144}Nd$ diagram (Fig. **F7**). On this diagram the trends are less well defined, which is to be expected since the $^{147}Sm/^{144}Nd$ ratios can be affected by various petrogenetic processes and may not directly reflect the mantle source composition. The eastern trend is dominated by Site 1160 samples, which define an almost flat trend with only a small decrease in $^{143}Nd/^{144}Nd$ ratios as $^{147}Sm/^{144}Nd$ ratios increase. Most glasses from other sites east of the 127°E Fracture Zone plot at the low $^{147}Sm/^{144}Nd$ end of this trend, with the exception of one sample from Site 1157 which plots below this trend. Samples from sites west of the 127°E Fracture Zone plot along a poorly defined trend of increasing $^{143}Nd/^{144}Nd$ with increasing $^{147}Sm/^{144}Nd$.

F5. Nd and Sm/Nd vs. distance from 126°E FZ, p. 17.

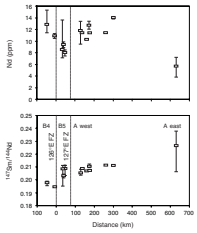

F6. $^{87}Sr/^{86}Sr$ and ε_{Nd} and $^{206}Pb/^{204}Pb$ and ε_{Hf}, p. 18.

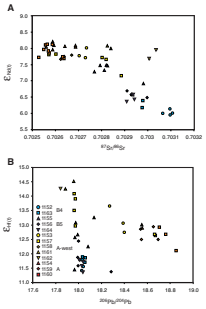

F7. $^{143}Nd/^{144}Nd$ and $^{147}Sm/^{144}Nd$, p. 19.

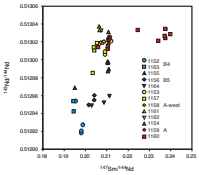

DISCUSSION

The major objective of Leg 187 was to constrain the history of the boundary between Indian and Pacific MORB mantle provinces as recorded by the isotopic signatures of lavas from old oceanic crust north of the AAD. Based on onboard trace element analyses, the shipboard scientific party concluded that the boundary has followed the depth anomaly (Christie, Pedersen, Miller, et al. 2001) as it has migrated westward at a rate of ~15 mm/yr relative to the spreading axis. Our data show that the boundary region is characterized by a gradual east-west increase in $^{87}Sr/^{86}Sr$, with a corresponding decrease in $^{143}Nd/^{144}Nd$ from Zone A-west, across Segment B5, into Segment B4. Leg 187 glasses define distinct eastern and western (Pacific and Indian) trends on the $^{87}Sr/^{86}Sr$ vs. $^{143}Nd/^{144}Nd$ diagram, with Site 1157 returning samples from both trends as well as their intersection. Lavas from eastern (Pacific) trend sites east of the 127°E Fracture Zone do not display any significant influence of the radiogenic Sr end-member that controls the western trend, and we see no sign of Indian MORB-source influence east of Zone A-west. The Sr-Nd isotopic composition of glasses therefore confirms the general conclusions derived by the Leg 187 shipboard scientific party in that the mantle boundary follows the depth anomaly.

Source End-Member Compositions and Mixing Relationships

The intersecting, linear trends in Sr-Nd isotope systematics and similar trends in Pb-Hf (Fig. F6) suggest that the basalts sampled during Leg 187 formed through the interaction of three contrasting source components. Sites 1160 and 1152, the easternmost and westernmost sites, respectively, represent two end-members. Sr and Nd isotopic compositions for Site 1160 are similar to those of Pacific-type axial samples from Zone A, whereas those of Site 1152 lavas are within the range of Indian-type axial samples from Zone B. The third end-member is distinguished from the two others by high $^{87}Sr/^{86}Sr$ combined with high ε_{Nd} (Fig. F6). This component appears to be most strongly expressed, and perhaps localized, in lavas from the Indian/Pacific boundary zone, within the eastern part of the depth anomaly (Sites 1161,1162, 1157, and 1153). We therefore refer to it as the boundary component. The boundary source has similar ε_{Nd} to the Pacific MORB source, similar $^{206}Pb/^{204}Pb$ to the Indian MORB source, and a wide range of $^{87}Sr/^{86}Sr$ values that are generally intermediate between those of the Indian and Pacific sources. ε_{Hf} is higher in the boundary source than in either the Indian or the Pacific MORB sources (Fig. F4).

The Sr-Nd and Pb-Hf isotope systematics described above appear to define coherent relationships among Leg 187 glasses, but they do not appear to account for the full variability of younger (0–7 Ma) lavas from the AAD (Figs. F8, F9) or from the broader SEIR region. This suggests that mantle source compositions for 14- to 28-Ma (Leg 187) lavas from the eastern AAD and Zone A were bounded by at least three localized, probably transient components: (1) a component that lies within the broad spectrum of Indian-type mantle compositions, (2) the boundary component, and (3) a Pacific-type mantle component. These three components are not, however, randomly intermixed, as they do not define the expected triangular fields in Sr-Nd and Pb-Hf isotope space. The Indian and the Pacific mantle sources do not seem to have interacted

F8. Along-axis $^{87}Sr/^{86}Sr$, ε_{Nd}, and $^{206}Pb/^{204}Pb$ with off-axis isotopic compositions, p. 20.

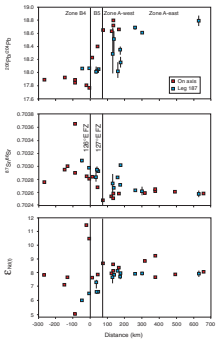

F9. Sr-Nd isotope systematics of on-axis and off-axis basalts, p. 21.

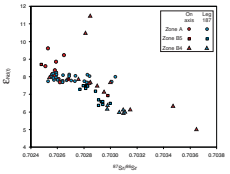

directly at this time. Rather, the intersecting linear trends defined by the Leg 187 glasses require that Pacific-type mantle interacted with the boundary component throughout Zone A-west, giving rise to the eastern trend, whereas Indian-type mantle interacted extensively with the boundary source primarily beneath Segment B5.

Compositional Variations across the Depth Anomaly

The AAD region is characterized by mantle regions of contrasting composition as well as marked along-axis variations in magmatic productivity. The geochemistry of the seafloor basalts must consequently reflect variations in both. Isotope dilution analyses of the Leg 187 glasses demonstrate systematic variations in REE concentrations across the depth anomaly (Fig. F5). The low Nd concentrations of Segment B5 glasses relative to glasses recovered west and east of this zone is the most marked feature and contrasts with Sr-Nd isotopic values that are intermediate between Zone B4 and Zone A-west glasses (Fig. F6). This contrast implies that the low Nd contents of Segment B5 glasses cannot be explained solely by variations in source composition.

The Nd contents increase from Zone A-east to Zone A-west, decrease westward into Zone B5, and increase again to Zone B4. This is accompanied by a decrease in Sm/Nd ratios from Zone A-east to Zone A-west and Zone B5 and a further decrease into Zone B4 (Fig. F5). In other words, the Nd concentrations decrease and the REE pattern becomes more light rare earth element (LREE) depleted eastward toward the 127°E Fracture Zone and Nd concentrations increase and REE patterns become slightly less LREE depleted westward toward the depth anomaly and the 127°E Fracture Zone.

This pattern may reflect eastward increase and westward decrease in the degree of melting toward the mantle boundary region in Zone A-west, compatible with a cooling of the Pacific mantle and a heating of the Indian mantle toward the mantle boundary region. This is consistent with several lines of evidence suggesting that the Pacific mantle east of the mantle boundary in the AAD region is warmer than the Indian mantle to the west (Christie et al., 1998), implying that the Pacific mantle would be conductively cooled and the Indian mantle heated toward the mantle boundary region.

Nature of the Boundary Component

The boundary component postulated above for Leg 187 lavas could represent a distinct mantle source localized to the boundary region or it may stem from small-scale heterogeneities present throughout the Pacific or the Indian MORB sources in the region. Such heterogeneities could either have been preferentially extracted in the region of the mantle boundary due to higher or lower degrees of melting, depending on the boundary component being the more fertile or the more refractory component of the heterogeneous source. The variations in elemental and isotopic compositions seem to be inconsistent with the boundary component being a dispersed heterogeneity in either the Pacific or the Indian mantle sources that are preferentially extracted in the boundary region. It therefore seems more likely that the boundary component represents a distinct mantle source that is associated with the boundary between the Pacific and the Indian MORB sources in the region.

The present data suggest that direct mixing between the Indian and the Pacific sources was restricted in Zone A-west at ~14–28 Ma and that these two primary MORB sources may have been spatially separated by the boundary source. Hole 1157A includes lavas of all three types (Pacific, Indian and boundary types). Only basaltic rubble was recovered from this hole (Christie, Pedersen, Miller, et al., 2001), suggesting that the samples may have been derived from a wider area than would be assumed for in situ lava flows, and it occurs in a region of oblique seafloor lineaments that may record an episode of rift propagation (Christie, Pedersen, Miller et al., 2001; **Christie et al.,** this volume). These observations suggest that the Pacific-type lavas may have been emplaced somewhat later than the Indian types. In any case, the isotopic variability of this hole demonstrates that interaction between Indian- and boundary-type sources also took place within Zone A-west.

The $^{206}Pb/^{204}Pb$ data for Leg 187 lavas (Kempton et al., 2002) show Indian-type values from Zone B4 across Zone B5 and a relatively narrow transition to Pacific-type values within Zone A-west (Fig. **F4**). In contrast, Nd, Sr, and Hf isotopes change systematically over ~250 km from Zone B4 to Zone A-west. This apparently contradictory evidence for the nature of the transition zone—abrupt or gradational—can be explained if two of our postulated sources, the Indian and boundary types have similar $^{206}Pb/^{204}Pb$ but different Nd, Hf, and Sr isotopic compositions. A mixing of the boundary source to the east with the Indian source and to the west across Zone B5 would result in the observed pattern with Indian $^{206}Pb/^{204}Pb$ values throughout Zone B5 and a gradual westward decrease in $^{87}Sr/^{86}Sr$ and increases in ε_{Nd} and ε_{Hf}.

The present data suggest that the three contrasting mantle sources were distributed and interacted in the following way:

1. An unequivocal Indian source was present beneath Segment B4 just west of the 126°E Fracture Zone.
2. This Indian MORB source mixed with the boundary source below Segment B5.
3. The boundary source interacted either with the Indian or the Pacific sources (but not with both in the same place) to yield the highly variable MORB population sampled in Zone A-west.
4. Only a Pacific-type source was present more than 250 km east of the 127°E Fracture Zone.

Comparison with On-Axis Samples—Evolution with Time

The boundary between Indian- and Pacific-type MORB mantle has been shown to be gradational along ~40 km within Segment B5-west terminating at the 126°E Fracture Zone (Pyle et al. 1992). Lavas dredged west of this fracture zone are unequivocally derived from an Indian MORB source, whereas lavas in Segment B5-east and Zone A are exclusively Pacific type (Pyle et al., 1992). The transition from Pacific to Indian MORB source within Segment B5-west is marked by a westward increase in $^{87}Sr/^{86}Sr$ and decreases in ε_{Nd} and $^{206}Pb/^{204}Pb$ ratios (Fig. **F8**).

Leg 187 lavas show comparable east-west changes with several notable features and differences (Fig. **F8**):

1. A marked increase in $^{206}Pb/^{204}Pb$, comparable to the on-axis change across the 126°E transform, occurs 100–150 km farther to the east in Zone A-west.
2. The off-axis east to west increase in $^{87}Sr/^{86}Sr$ occurs over a greater distance and begins more than 100 km farther east within Zone A-west.
3. In both cases, changes in Sr isotopic compositions are more gradational than the corresponding changes in $^{206}Pb/^{204}Pb$.
4. The east to west decrease in Nd isotopic compositions is more marked off-axis than on-axis.
5. The extreme local variability in Nd isotopes in Zone B4 on-axis is not documented off-axis, but Nd isotopic variability off-axis is greatest in Zone A-west.

The two contrasting trends shown by the Leg 187 glasses in Sr-Nd isotope space (Fig. **F6**) are not shown by basalts dredged at the spreading axis (Fig. **F8**). Excluding two data points with unusual high Nd isotopic compositions from Zone B4, the on-axis basalts define a broad trend from Pacific compositions in Zone A to Indian compositions in Zone B4. The boundary component seems not to be present at the axis, and it appears therefore that the mantle region with time may have changed from a three-component system to a two-component system. Kempton et al. (2002) documented that basalts with high ε_{Hf} (>12) are abundant west of the 126°E Fracture Zone at the axis and suggested that the mantle region present below Zone A-west had expanded with time. The Sr-Nd isotope systematics of on- and off-axis basalts (Fig. **F9**) cannot be explained by an expansion of the boundary component. However, the gradual boundary between the Indian mantle source and the boundary component off-axis across Zone B5 (Fig. **F4**) suggest that the two separate source regions mixed. It is therefore possible that the change from three- to a two-component system in Sr-Nd isotopic space may reflect a gradual mixing of the boundary source with the Indian source present below Zone B4 with time.

Origin of the Boundary Component

Nd and Sr isotopic ratios are generally inversely correlated in magmatic rocks that show primary isotopic variations for these elements. Increases in $^{87}Sr/^{86}Sr$ without corresponding changes in $^{143}Nd/^{144}Nd$, as shown by glasses from Leg 187 sites within Zone A (Fig. **F6**), are, however, typical for seafloor basalts that have been variably altered by rock-seawater interaction. Superficially, the Zone A trend, which is of this type, could be interpreted as reflecting variable low-temperature alteration. It can not be excluded that the glasses analyzed from Site 1162 show the effect of low-temperature alteration since the quality of the glasses was not the best (contained spherulites). The glasses analyzed from Sites 1153, 1161, and 1157, which define the high $^{87}Sr/^{86}Sr$ end of the eastern trend if Site 1162 is excluded, were all of good quality. It seems therefore unlikely that eastern trend may be explained by variable low-temperature alteration. This is supported by that basalts from Sites 1161, 1162, and 1157 also show end-member compositions in Pb-Hf space (Fig. **F6**) (Kempton et al., 2002). We conclude that the flat trends reflect unusual mantle isotope systematics and therefore that they may provide insight into the origin of the depth anomaly.

Selective enrichment in $^{87}Sr/^{86}Sr$ that is not coupled with a corresponding decrease in $^{143}Nd/^{144}Nd$ has been observed in immature island

arc basalts, probably reflecting selective enrichment of the mantle wedge by radiogenic Sr derived from subducted seawater. Gurnis et al. (1998) suggested that the AAD may be located over an old subduction zone that existed between the Pacific plate and the eastern margin of Gondwanaland up until the Early Cretaceous and was subsequently overridden by the Australian and Antarctic plates as they drifted eastward. This is to some extent supported by the fact that $^{3}He/^{4}He$ ratios measured in basalts from the AAD region are among the lowest values yet observed in MORBs away from the influence of subduction zones.

Kempton et al. (2002) adopted the model by Gurnis et al. (1998) to explain the isotopic boundary in the AAD region and argued that basalts with high ε_{Hf} values found within Zone A-west could have been derived from a subduction-modified mantle. They suggested a two-stage process, with an initial step that led to a decrease in $^{143}Nd/^{144}Nd$ ratios and an increase in Lu/Hf ratios due to enrichment of the mantle wedge in REE relative to high field strength elements (HFSE). Subsequent ingrowths of radiogenic Hf and Nd isotopes result in an increase in ε_{Hf} above that of the Pacific source and a similar or retarded growth of radiogenic Nd.

The lavas suggested by Kempton et al. (2002) to have been derived from a subduction-modified Pacific mantle (termed the boundary component in this paper) are here documented to have similar Nd isotopic ratios, similar Nd contents, and similar Sm/Nd ratios as lavas derived from the nearby Pacific source. The decrease in $^{143}Nd/^{144}Nd$ postulated to have taken place during initial subduction modification by Kempton et al. (2002) must have been accompanied or followed by an increase in Sm/Nd ratios in order for the two source regions now to show similar Nd isotopic compositions. The similar Nd contents and Sm/Nd ratios of lavas derived from the two sources does not support such a LREE depletion. A lack of subduction signatures in the trace element patterns of lavas derived from the presumed subduction-modified Pacific mantle source (Kempton et al., 2002) is consistent with this. We therefore conclude that the origin of the boundary component remains an open question.

Significance of Local Variability in Isotopic Compositions

The AAD is characterized by large regional variations in isotopic compositions. The analyses of the cores recovered during Leg 187 also demonstrate large local variability in isotopic compositions in the region. The shallow penetration into the volcanic basement and the poor recovery suggest that the total variability in the vicinity of any given site could be larger than that reported here. Despite the limited sampling, several holes show variability of up to 30% of the regional range in Nd isotopic ratios (Fig. **F4**). The largest local variability is present within Zone A-west, where Sr and Nd isotopic ratios in individual holes vary by as much as 54% and 30%, respectively, of the regional range. This large local variability demonstrates that there is significant local mantle heterogeneity across Zone A-west, and that the magma extraction processes in this region were unable to homogenize these isotopic contrasts. The latter restriction seems to preclude the presence either of long-lived magma reservoirs or of extensive mush zones through which magma must migrate. These conclusions are consistent with large local

variability observed in the basaltic sequence drilled in Ocean Drilling Program Hole 504B (Pedersen and Furnes, 2001).

ACKNOWLEDGMENTS

This research used samples and data provided by the Ocean Drilling Program (ODP). ODP is sponsored by the U.S. National Science Foundation (NSF) and participating countries under management of Joint Oceanographic Institutions (JOI), Inc. Funding for this research was provided by the Norwegian Research Council through the SUBMAR program. J. Alt and H. Paulick are thanked for constructive reviews of the manuscript.

REFERENCES

Christie, D.M., Pedersen, R.B., Miller, D.J., et al., 2001. *Proc. ODP, Init. Repts.,* 187 [Online]. Available from World Wide Web: <http://www-odp.tamu.edu/publications/187_IR/187ir.htm>. [Cited 2003-09-15]

Christie, D.M., West, B.P., Pyle, D.G., and Hanan, B.B., 1998. Chaotic topography, mantle flow and mantle migration in the Australian–Antarctic discordance. *Nature,* 394:637–644.

Forsyth, D.W., Ehrenbard, R.L., and Chapin, S., 1987. Anomalous upper mantle beneath the Australian–Antarctic discordance. *Earth Planet. Sci. Lett.,* 84:471–478.

Gurnis, M., Muller, R.D., and Moresi, L., 1998. Cretaceous vertical motion of Australia and the Australian–Antarctic Discordance. *Science,* 279:1499–1504.

Hamelin, B., and Allègre, C.-J., 1985. Large-scale regional units in the depleted upper mantle revealed by an isotope study of the South-West Indian Ridge. *Nature,* 315:196–199.

Kempton, P.D., Pearce, J.A., Barry, T., Fitton, J.G., Langmuir, C., and Christie, D.M., 2002. Sr-Nd-Pb-Hf isotope results from ODP Leg 187: evidence for mantle dynamics of the Australian–Antarctic discordance and origin of Indian MORB source. *Geochem., Geophys., Geosyst.,* 3:10.1029/2002GC000320.

Klein, E.M., Langmuir, C.H., Zindler, A., Staudigel, H., and Hamelin, B., 1988. Isotope evidence of a mantle convection boundary at the Australian–Antarctic Discordance. *Nature,* 333:623–629.

Mahoney, J.J., le Roex, A.P., Peng, Z., Fisher, R.L., and Natland, J.H., 1992. Southwestern limits of the Indian Ocean Ridge mantle and the origin of low $^{206}Pb/^{204}Pb$ mid-ocean ridge basalts: isotope systematics of the central Southwest Indian Ridge (17°–50°E). *J. Geophys. Res.,* 97:19771–19790.

Mahoney, J.J., White, W.M., Upton, B.G.J., Neal, C.R., and Scrutton, R.A., 1996. Beyond EM-1: lavas from Afanasy-Nikitin Rise and the Crozet archipelago, Indian Ocean. *Geology,* 24:615–618.

Marks, K.M., Sandwell, D.T., Vogt, P.R., and Hall, S.A., 1991. Mantle downwelling beneath the Australian–Antarctic Discordance Zone: evidence from geoid height versus topography. *Earth Planet. Sci. Lett.,* 103:325–338.

Marks, K.M., Vogt, P.R., and Hall, S.A., 1990. Residual depth anomalies and the origin of the Australian–Antarctic Discordance Zone. *J. Geophys. Res.,* 95:17325–17337.

Pedersen, R.B., and Furnes, H., 2001. Nd- and Pb-isotopic variations through the upper oceanic crust in DSDP/ODP Hole 504B, Costa Rica Rift. *Earth Planet. Sci. Lett.,* 189:221–235.

Pyle, D.G., 1994. Geochemistry of mid-ocean-ridge basalt within and surrounding the Australian–Antarctic Discordance [Ph.D. dissert.]. Oregon State Univ., Corvallis.

Pyle, D.G., Christie, D.M., and Mahoney, J.J., 1990. Upper mantle flow in the Australian–Antarctic Discordance. *Eos, Trans. Am. Geophys. Union,* 71:1388. (Abstract)

Pyle, D.G., Christie, D.M., and Mahoney, J.J., 1992. Resolving an isotopic boundary within the Australian–Antarctic Discordance. *Earth Planet. Sci. Lett.,* 112:161–178.

Vogt, P.R., Cherkis, N.Z., and Morgan, G.A., 1983. Project investigator—1. Evolution of the Australia–Antarctic Discordance deduced from a detailed aeromagnetic study. *In* Oliver, R.L., James, P.R., and Jago, J.B. (Eds.), *Antarctic Earth Science*. Antarct. Earth Sci., [Pap.—Int. Symp.], 4th, 608–613.

Weissel, J.K., and Hayes, D.E., 1971. Asymmetric seafloor spreading south of Australia. *Nature,* 231:518–522.

Figure F1. Regional map of the Southern Ocean showing the setting of the Australian Antarctic Discordance (AAD) and the region sampled during Leg 187.

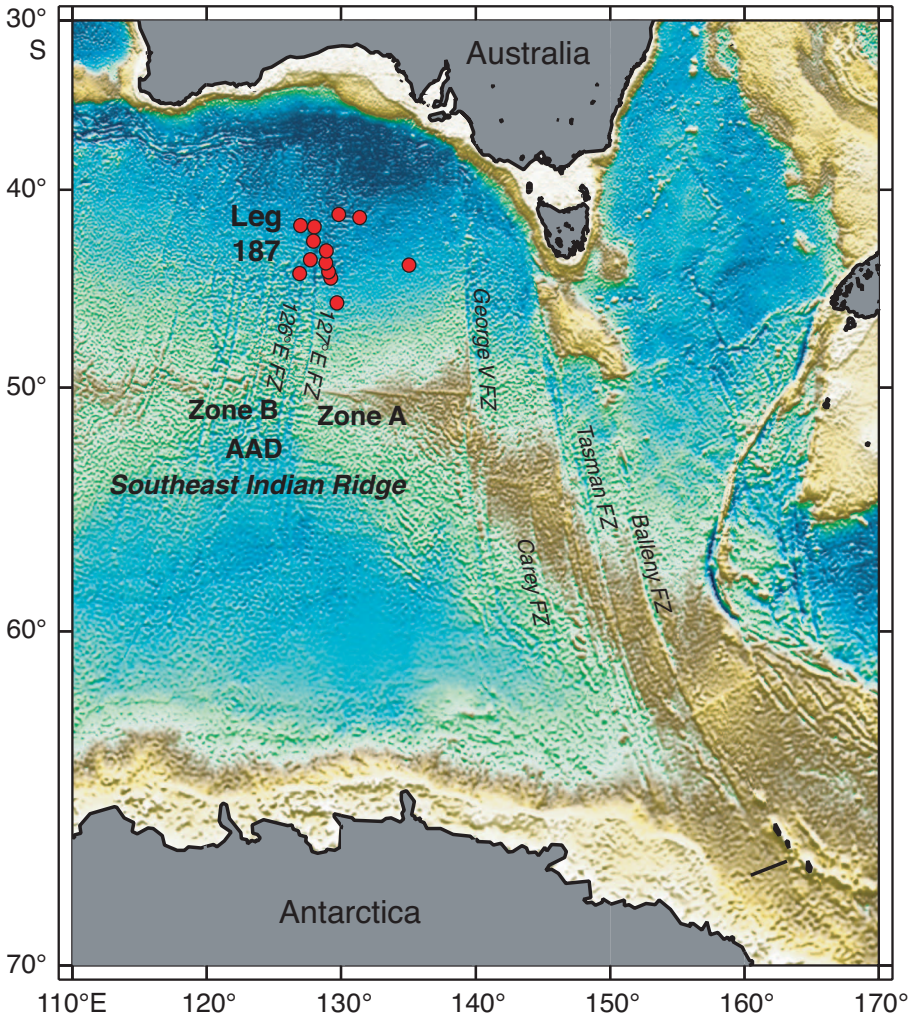

Figure F2. Leg 187 site locations in relation to the residual depth anomaly (gray contours) and SeaBeam bathymetry (modified from Christie, Pedersen, Miller, et al., 2001).

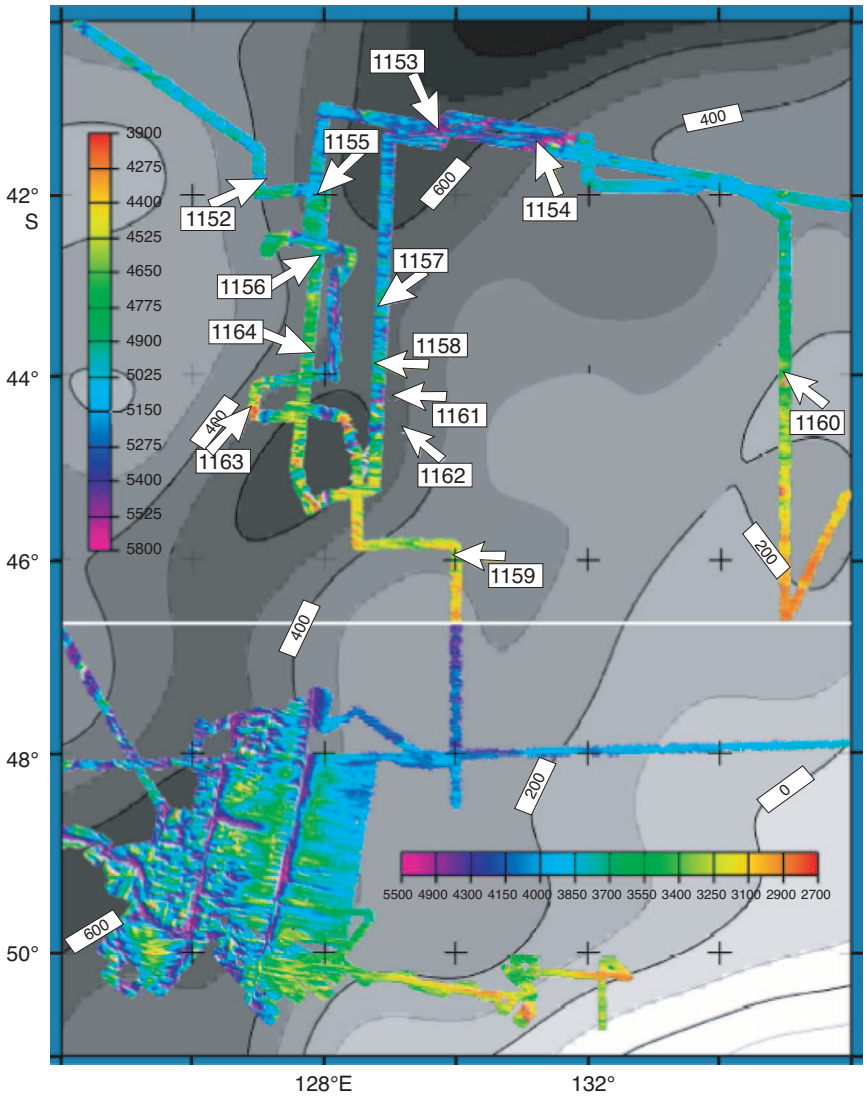

Figure F3. Leg 187 site locations in relation to seafloor isochrons (after Vogt et al., 1983) (modified from Christie, Pedersen, Miller, et al., 2001). FZ = fracture zone.

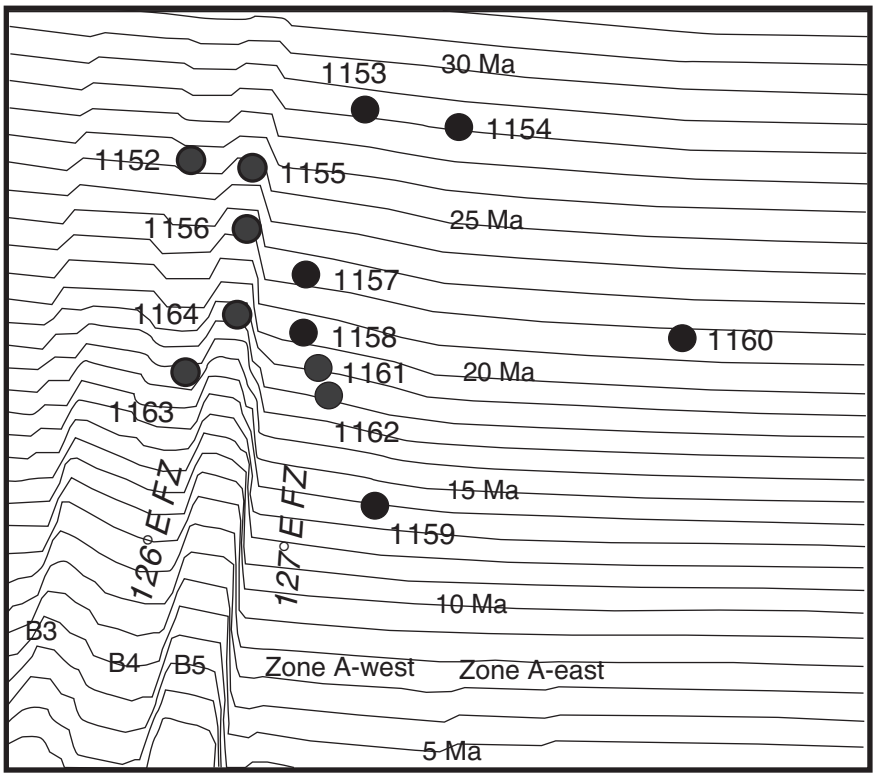

Figure F4. Diagram showing maximum, the minimum, and average $^{87}Sr/^{86}Sr$, ε_{Nd}, ε_{Hf}, and $^{206}Pb/^{204}Pb$ values. For each site the isotopic data have been plotted against the distance between the sites and the 126°E Fracture Zone (FZ) (measured perpendicular to the fracture zone, i.e. parallel with the spreading ridge). Pb and Hf isotopic data are from Kempton et al. (2002).

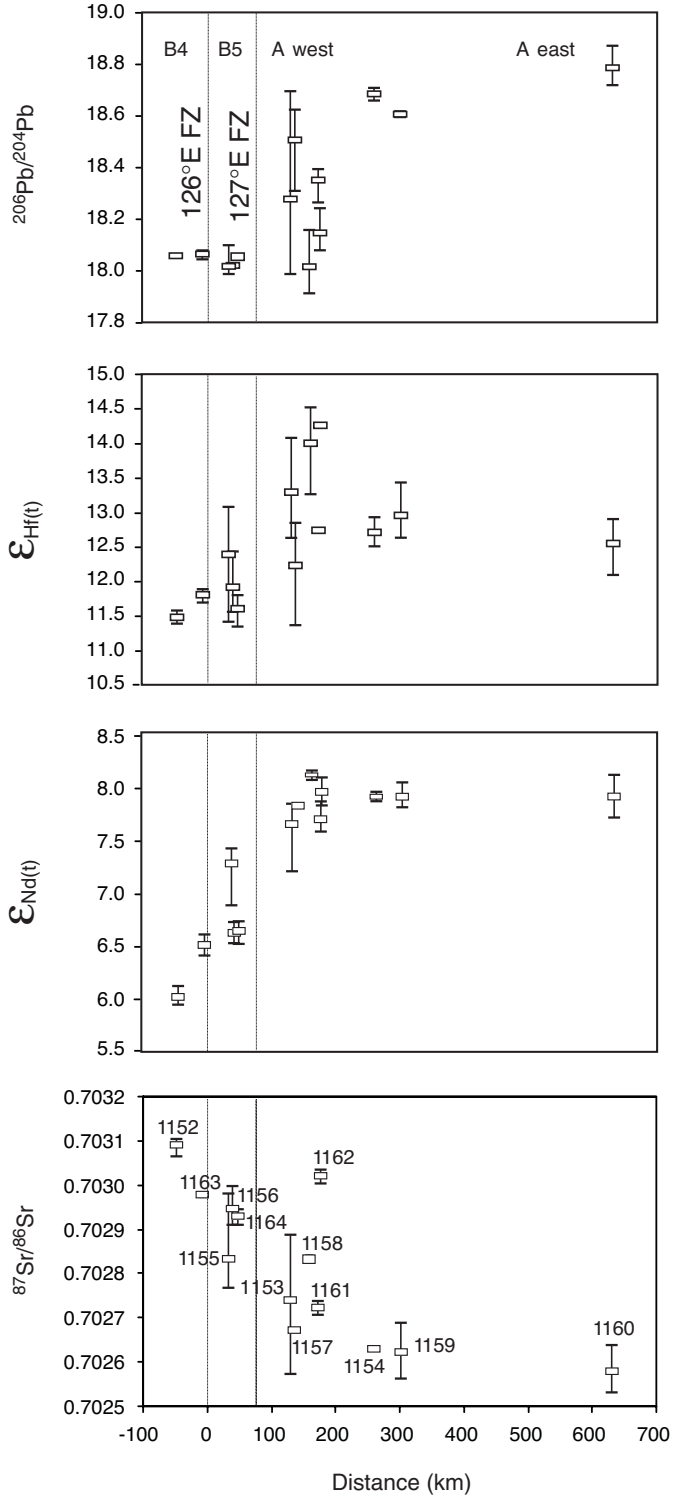

Figure F5. Variations in Nd and Sm/Nd ratios in Leg 187 glasses plotted against distance from the 126°E Fracture Zone (FZ).

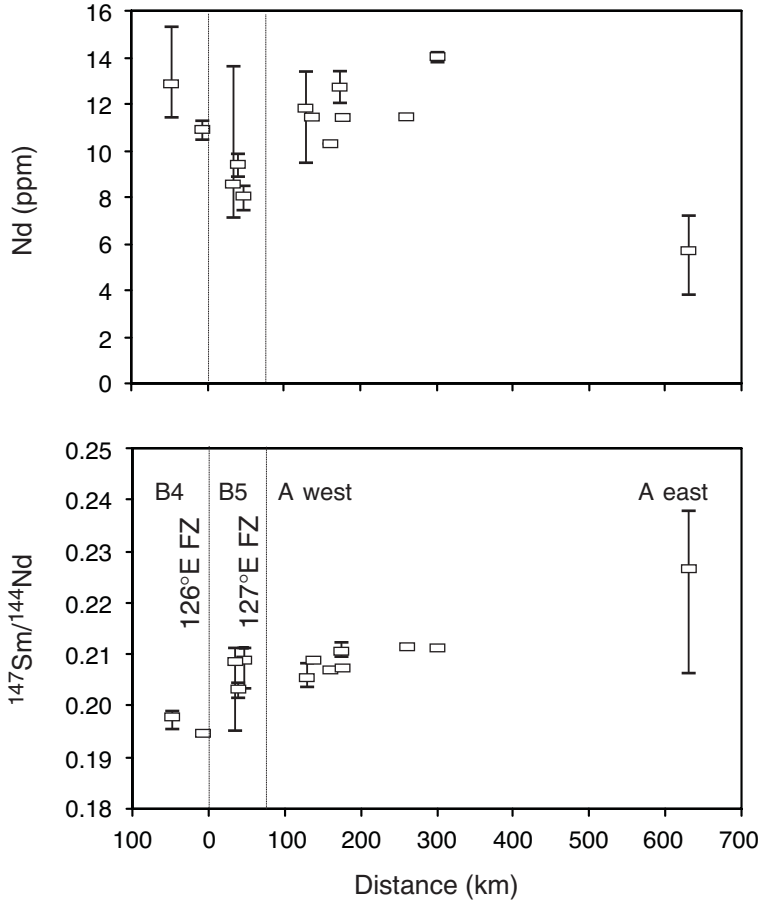

Figure F6. Diagram illustrating covariations between (**A**) $^{87}Sr/^{86}Sr$ and ε_{Nd} (data from this study), and (**B**) $^{206}Pb/^{204}Pb$ and ε_{Hf} (data from Kempton et al., 2002). Note the two trends primarily defined by sites west and east of the 127°E Fracture Zone (FZ) (western and eastern trends).

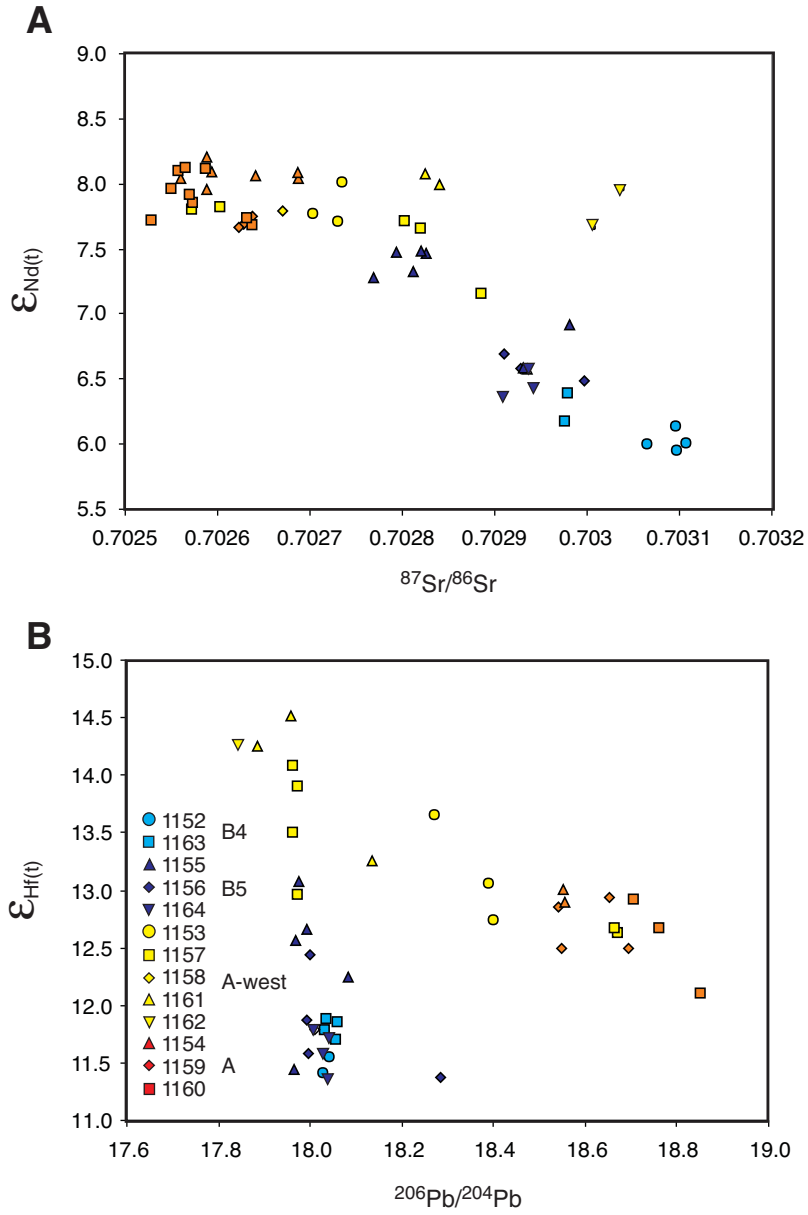

Figure F7. Diagram showing covariations $^{143}Nd/^{144}Nd$ and $^{147}Sm/^{144}Nd$. See text for discussion.

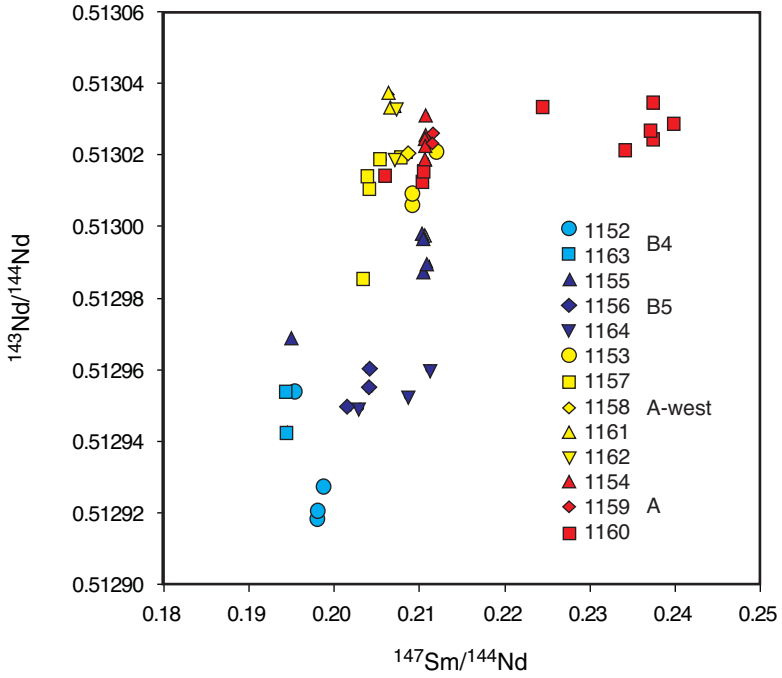

Figure F8. Comparison of along-axis variations in $^{87}Sr/^{86}Sr$, ε_{Nd}, and $^{206}Pb/^{204}Pb$ with off-axis isotopic composition at Leg 187 sites. The isotopic compositions have been plotted against the distance between sample locations and the 126°E Fracture Zone (FZ) (the distances were measured perpendicular to the fracture zone, i.e., parallel with the spreading ridge). On-axis data from Pyle et al. (1992), Leg 187 data from this study and Kempton et al. (2002).

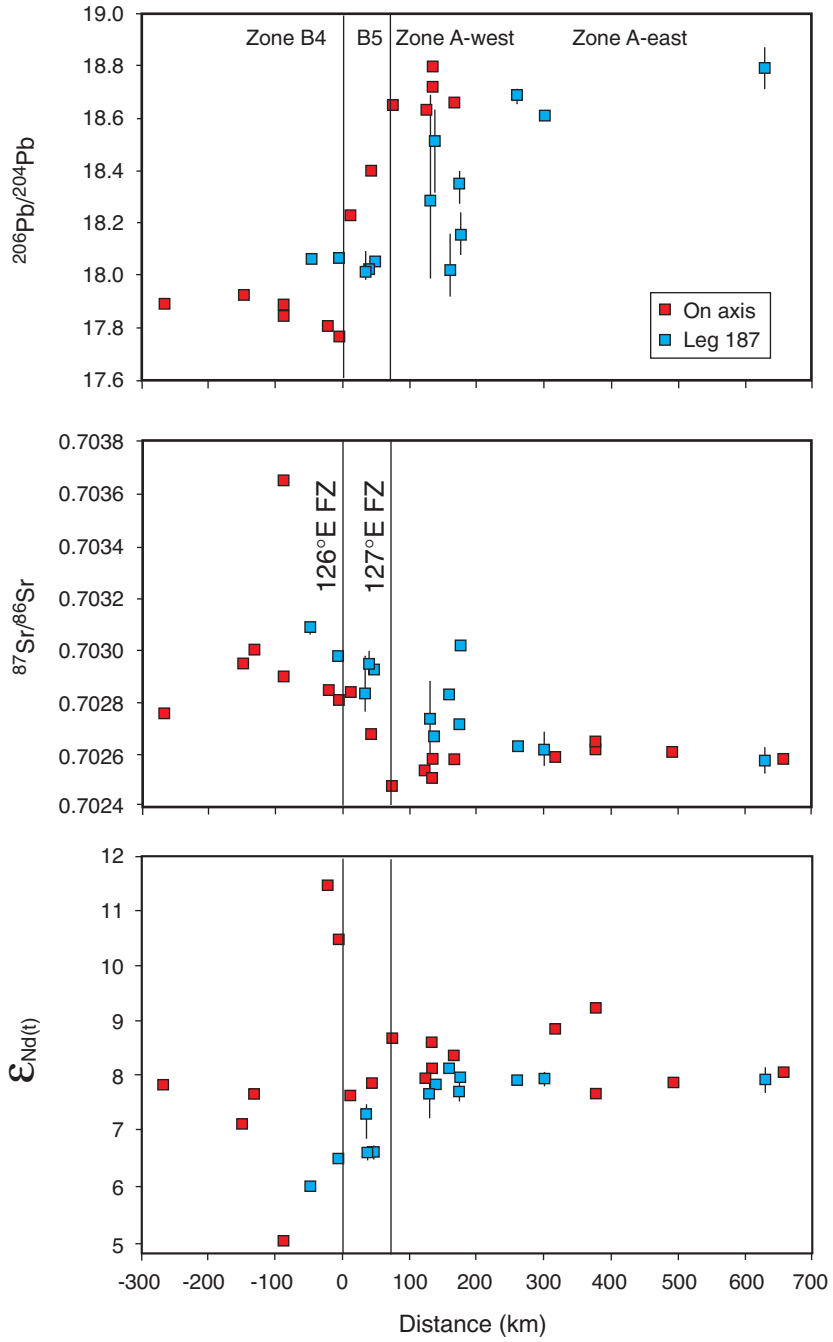

Figure F9. Comparison of Sr-Nd isotope systematics of on-axis and off-axis (Leg 187) basalts. Note that the two well-defined trends defined by the Leg 187 glasses are not evident in on-axis samples. See text for further discussion. On-axis data from Pyle et al. (1992).

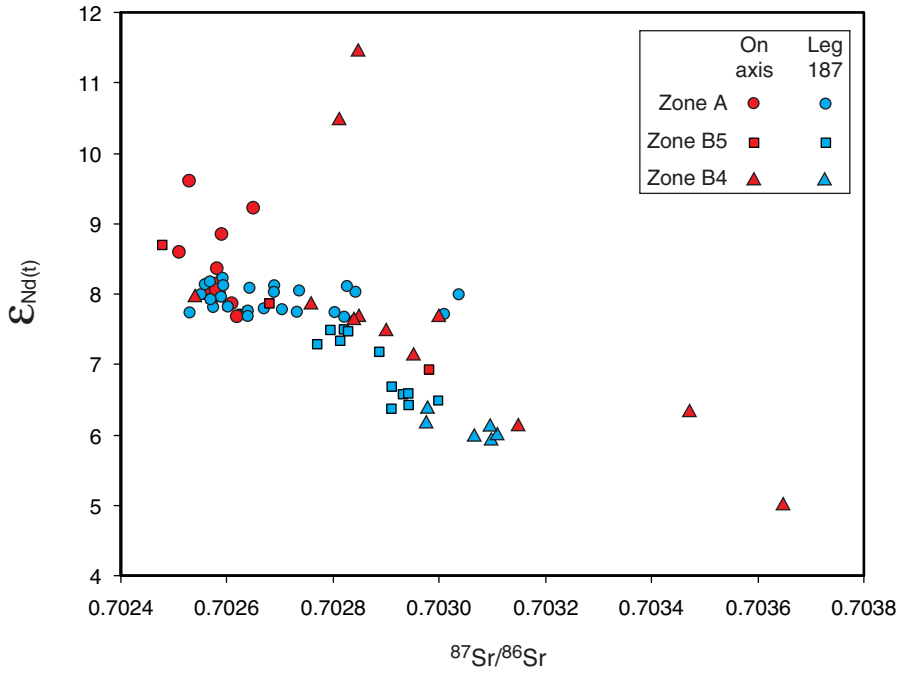

Table T1. Nd and Sr isotopic compositions, and Nd and Sm concentrations of Leg 187 glasses. (Continued on next page.)

Core, section, interval (cm)	$^{87}Sr/^{86}Sr$	±	$^{143}Nd/^{144}Nd$	±	$^{147}Sm/^{144}Nd$	Sm (ppm)	Nd (ppm)	ε_{Nd}
187-1152A-								
1R-1, 60–62	0.70312	8	0.512954	6	0.195	4.92	15.23	6.17
187-1152B-								
3R-1, 2–4	0.703105	8	0.512962	10	0.199	3.75	11.41	6.32
5R-1, 68–74	0.703074	8	0.512955	7	0.198	3.90	11.89	6.18
5R-1, 142–143	0.703095	9	0.512953	6	0.198	4.17	12.72	6.14
187-1153A-								
7W-4, 60–65	0.702745	8	0.51306	6	0.212	4.67	13.32	8.23
8R-1, 20–26	0.702742	9	0.513045	6	0.209	4.37	12.62	7.93
8R-1, 100–105	0.702717	8	0.513047	6	0.209	4.15	11.99	7.99
187-1154A-								
2R-1, 31–37	0.702699	9	0.513061	7	0.211	4.83	13.83	8.25
3R-1, 93–96	0.702572	7	0.513061	6	0.211	4.93	14.12	8.25
3R-2, 43–46	0.702605	8	0.513063	7	0.211	4.93	14.14	8.30
4R-1, 69–73	0.702652	9	0.513062	7	0.211	4.87	13.94	8.27
4R-2, 41–44	0.702601	8	0.513069	6	0.211	4.85	13.89	8.41
6R-1, 6–11	0.702699	8	0.513063	6	0.211	4.91	14.08	8.28
7R-1, 0–8	0.702601	9	0.513057	7	0.211	4.79	13.72	8.17
187-1155A-								
5R-1, 20–23	0.702987	8	0.513001	7	0.195	4.38	13.59	7.08
187-1155B-								
2R-1, 55–57	0.702833	9	0.513031	6	0.211	2.68	7.70	7.67
2R-1, 66–68	0.702776	9	0.513021	7	0.211	2.47	7.10	7.48
3R-1, 38–43	0.702829	9	0.513032	6	0.211	2.68	7.69	7.69
5R-1, 34–38	0.702801	9	0.513031	6	0.211	2.64	7.58	7.68
9R-2, 19–22	0.702819	9	0.513024	7	0.211	2.65	7.60	7.53
187-1156A-								
2R-3, 133–136	0.702933	8	0.512985	6	0.204	3.17	9.38	6.78
3R-1, 102–104	0.702915	8	0.512991	6	0.204	2.99	8.85	6.89
187-1156B-								
4R-1, 102–106	0.703003	8	0.51298	6	0.202	3.26	9.78	6.67
187-1157A-								
1W-CC, 13–17	0.702894	9	0.513015	7	0.204	3.18	9.43	7.35
3R-1, 20–24	0.702613	9	0.513049	6	0.208	4.58	13.32	8.03
3R-1, 25–29	0.70258	9	0.513048	7	0.206	4.54	13.36	8.00
187-1157B-								
2R-1, 55–56	0.70283	9	0.51304	6	0.204	3.99	11.80	7.84
4R-1, 136–138	0.702813	9	0.513043	6	0.204	3.69	10.93	7.90
4R-1, 34–38	0.702679	9	0.513047	7	0.209	3.94	11.42	7.98
187-1159A-								
6R-2, 55–57	0.702633	9	0.513042	6	0.212	3.98	11.38	7.89
7R-1, 139–141	0.702642	7	0.513045	7	0.212	3.98	11.39	7.94
7R-2, 16–17	0.702628	9	0.513041	6	0.212	3.98	11.37	7.86
187-1160A-								
3R-1, 19–21	0.702533	9	0.513044	11	0.206	1.48	4.35	7.92
187-1160B-								
1W-1, 8–14	0.702576	9	0.513055	7	0.234	2.27	5.84	8.13
3R-1, 7–16	0.702563	9	0.513066	6	0.225	1.56	4.19	8.34
6R-2, 5–8	0.702641	9	0.513043	6	0.211	2.48	7.13	7.90
6R-2, 96–98	0.702569	8	0.513069	9	0.238	2.44	6.22	8.40
7R-1, 9–11	0.702634	8	0.513046	6	0.211	2.50	7.18	7.95
8R-1, 20–22	0.702573	9	0.513058	7	0.238	2.44	6.21	8.20
9R-1, 5–7	0.702551	9	0.513061	8	0.237	1.49	3.80	8.25
9R-1, 70–74	0.702591	8	0.513069	6	0.238	2.45	6.23	8.40
187-1161A-								
3R-1, 8–9	0.702851	9	0.513057	6	0.207	3.51	10.28	8.17
3R-1,68–69	0.702837	9	0.513061	6	0.207	3.52	10.29	8.25
187-1162B-								
8R-1, 80–82	0.703014	8	0.513042	6	0.207	3.88	11.30	7.88
8R-1, 80–84	0.703044	9	0.513056	7				
187-1163A-								

Table T1 (continued).

Core, section, interval (cm)	$^{87}Sr/^{86}Sr$	±	$^{143}Nd/^{144}Nd$	±	$^{147}Sm/^{144}Nd$	Sm (ppm)	Nd (ppm)	ε_{Nd}
8R-1, 41–43	0.702983	8	0.512975	6	0.194	3.35	10.41	6.57
9R-2, 0–2	0.702979	8	0.512963	6	0.195	3.63	11.27	6.35
187-1164A-								
2R-1, 1–5	0.702912	9	0.512975	6	0.203	2.69	8.00	6.57
187-1164B-								
1W-CC, 23–25	0.702945	9	0.512979	6	0.209	2.91	8.43	6.65
4R-2, 135–138	0.702939	9	0.512986	6	0.211	2.59	7.41	6.80
8R-1, 36–39	0.702934	9	0.512987	6	0.211	2.86	8.20	6.80